

Mapping atomistic to coarse-grained polymer models using automatic simplex optimization to fit structural properties

Dirk Reith*, Hendrik Meyer and Florian Müller-Plathe

Max-Planck-Institut für Polymerforschung, Ackermannweg 10, D-55128 Mainz, Germany

(October 25, 2018)

Abstract

We develop coarse-grained force fields for poly (vinyl alcohol) and poly (acrylic acid) oligomers. In both cases, one monomer is mapped onto a coarse-grained bead. The new force fields are designed to match structural properties such as radial distribution functions of various kinds derived by atomistic simulations of these polymers. The mapping is therefore constructed in a way to take into account as much atomistic information as possible. On the technical side, our approach consists of a simplex algorithm which is used to optimize automatically non-bonded parameters as well as bonded parameters. Besides their similar conformation (only the functional side group differs), poly (acrylic acid) was chosen to be in aqueous solution in contrast to a poly (vinyl alcohol) melt. For poly (vinyl alcohol) a non-optimized bond angle potential turns out to be sufficient in connection with a special, optimized non-bonded potential. No torsional potential has to be applied here. For poly (acrylic acid), we show that each peak of the radial distribution function is usually dominated by some specific model parameter(s). Optimization of the bond angle parameters is essential. The coarse-grained forcefield reproduces the radius of gyration R_G of the atomistic model. As a first application, we use the force field to simulate longer chains and compare the hydrodynamic radius R_H with experimental data.

I. INTRODUCTION

Many computer simulations of polymers suffer from the detailed treatment of the fast modes (e.g. bond vibrations) on the microscopic length scale: It has the serious consequence that the time propagation of the system can only be performed in tiny steps. Even the application of supercomputers can not overcome the essential problem that the total simulated time of the system is typically limited to the order of nanoseconds. Consequently, the slow modes

*corresponding author, email: reith@mpip-mainz.mpg.de

(e.g. radius of gyration or end-to-end vector) can hardly be equilibrated. It is therefore not feasible to perform fully detailed atomistic simulations in order to derive specific macroscopic bulk properties of polymers. The study of realistically large atomistic systems is far from being feasible. [1]

This study is geared to the question of how to enhance size and simulated real time of a polymer system in computer simulations. Observe that we refer to specific polymer systems with detailed information on the atomistic length scale, not just to generic Gaussian chains. Such an enhancement would especially be useful if the resulting simulations would still keep an essential part of the atomistic information of the system.

In recent years, various so-called coarse-graining (CG) methods have been developed to enhance polymer simulations. They are very different in spirit and purpose. Some examples are the ‘time coarse graining’, [2] lattice approaches like the bond fluctuation model, [3–5] or the high coordination lattice. [6, 7] On a larger length scale, dissipative particle dynamics (DPD) and smoothed particle dynamics (SPD) are frequently used to tackle hydrodynamic problems. [8, 9]

With our approach, we map the atomistic system with its detailed chemistry to a coarser, mesoscopic model. This is done in continuous space. The crucial point is to incorporate the neglected atomistic degrees of freedom in some way into the coarse-grained model. The coarse-grained monomers are therefore designed such that they can be identified with specific chemical groups of the polymer itself (as an example, cf. Fig. 1). To gain the adequate “local” structure, we have to construct suitable intra-molecular potential terms. For the “global” structure of a polymer, the non-bonded interactions play a major role and, hence, they also have to be adjusted correctly. To do so, we first have to calculate the appropriate bond length, angular and torsional statistics of the atomistic simulations. For the fitting procedure, we adapted our simplex optimization algorithm which was originally implemented for the development of atomistic force fields. [10] This procedure was already successfully applied for coarse graining protocols of dense molecular liquids such as diphenyl carbonate or tetrahydrofuran. [11]

In this contribution, we extend the optimization against structural properties to vinyl polymers. For diversity, we chose a melt of poly (vinyl alcohol) (PVA) and an aqueous solution of poly (acrylic acid) (PAA) in form of its sodium salt. We show explicitly how to derive the coarse grained force fields starting from atomistic simulation data. All parametrizations as well as the most important steps of the simplex optimization are given. We focus on the interplay of various parameters and discuss some technical problems we had to overcome in the course of the optimization process. A first comparison with experimental data validates finally the usefulness of the coarse-grained PAA force field.

II. METHODS

A. Conceptual

Potentials for coarse-grained (CG) polymers may not only incorporate energetic, i.e. local aspects of the underlying microscopic model. Due to many-body effects, they also have to account for the entropic contributions from the conformational degrees of freedom of the chain. Therefore, we utilize structural information like intra- and inter-chain distribution functions which contain the entropic information as target functions to construct our CG force field.

We start from the approach used by Tschöp et al. for the simulation of polycarbonate (PC) melts. [12,13] They assumed that the distribution functions for length, angles and torsions taken between the coarse-grained beads directly factorize into independent distribution functions of the above variables. This worked reasonably well: It was tested for three different PC modifications. After remapping to an atomistic model, the resulting microscopic structure compared well to neutron scattering data. [14] The main difference to our course of action is, that they derived their torsional distributions via quantum chemistry calculations. Without any fitting procedure, they then assumed the Boltzmann-inverted functions as potentials for their force fields.

By contrast, we consider the construction of the force field as a so-called inverse problem: find an interparticle potential which reproduces a given radial distribution function (RDF) or set of RDFs. The latter have proven to be suitable target functions in the case of simple liquids. [11] For polymer chains modifications originating from the connectivity are necessary: We use partial RDFs, the so called RDF-a and RDF-b, as additional target functions. The first refers to an intrachain RDF for which we ignored the nearest neighbour chain particles. This can be easily done in computer simulations. The latter denotes the intrachain RDF excluding the two next neighbours.

To perform an automatic optimization, we need three technical ingredients: (i) specification of the potentials and parameters to be optimized, (ii) evaluation of the quality of the total test potential, i.e. a merit function defining a hypersurface in the parameter space which has to be minimized, and (iii) rules to modify the test potential to find a better fit of the target function. While the latter two points are rather technical and easy to implement, the specification of the functional form of the inter-particle potentials turns out to be the most difficult part. For details on the simplex optimization scheme as we use it we refer to Refs. 10 and 11.

Atomistic polymer force fields are usually decomposed into two main parts: bonded and non-bonded potential. For both there are several terms contributing which describe the energy required for distorting the polymer in a specific fashion. In general, the total force field energy can then be written as follows.

$$\begin{aligned} V_{tot} &= V_{bonded} + V_{nb} \\ &= (V_{str} + V_{bend} + V_{tors}) + (V_{vdw} + V_{es}) \end{aligned} \tag{2.1}$$

V_{str} is the potential accounting for the bond stretching between two atoms, V_{bend} the energy needed for bending a bond angle, V_{tors} represents the torsional energy, V_{vdw} accounts for the excluded volume repulsive as well as the London attractive forces between atoms and

V_{es} finally describes the electrostatic interactions. The coarse-grained force field shall be designed in the same way. However, having so many potential terms in mind, it is not meaningful trying to optimize them all at the same time. Instead, a more viable way to proceed is the successive adjustment of the terms, in the order of their relative strength.

$$V_{str} \rightarrow V_{bend} \rightarrow V_{vdw} \rightarrow V_{tors} \quad (2.2)$$

Disregarding V_{es} , Scheme (2.2) illustrates the relative rigidity of the force field terms, assuming that V_{vdw} is switched off for two adjacent atoms next to an arbitrary atom in a polymer chain. Therefore, it makes no sense, e.g., to optimize V_{vdw} if V_{str} has an inappropriate shape. We will, hence, start with the stretching energy, working our way systematically down to the torsional energy.

The implementation is performed differently for PVA and PAA, respectively. We present them in the subsequent Section III. Note that we do not consider electrostatic forces in our force fields. In the case of poly (vinyl alcohol), this is clearly justified because it represents a neutral polymer. For the (fully) deprotonated poly (acrylic acid), one has to be very careful. Taking away the explicit treatment of the charges implies, that the force field we develop can not be applied to derive some specific properties of PAA. Especially dynamical properties can not be expected to be calculated correctly. However, if concentrating on static properties and the fact that we want to focus on the entropic contributions of the free energy, our approach is still meaningful, as we will point out in Section III B 1.

B. Computational

All simulations are performed in the NVT ensemble. The system consists of an orthorhombic box employing periodic boundary conditions. The Langevin equations of motion are integrated by the velocity Verlet algorithm with a time step $\Delta t = 0.01\tau$. [15] (Brownian Dynamics is assumed to be most appropriate for our mean-field type coarse-graining simulations.) For technical reasons the potentials are normalized such that a temperature of $k_B T = 1$ is achieved. This temperature is maintained by the Langevin-thermostat with friction constant $\Gamma = 0.5\tau^{-1}$. [16]

Starting configurations are generated as random walks according to the given bond length, bond angle and torsion angle statistics (for the isolated chain). The chains are then randomly placed into the simulation box, taking into account periodic boundary conditions. The chains will now have some strong overlaps. To avoid excluded volume problems, the non-bonded potential is, hence, switched on slowly. That allows the chains to relax the overlaps smoothly.

We equilibrate our polymer systems as follows: Either, we use a newly generated start configuration or, which represents the regular way, we take the last configuration of a previous run. A pre-equilibration procedure follows (a few thousand simulation steps with very short time interval). Here, we apply an artificial upper bound to the forces to relax overlapping monomers in a well controlled way. This can be necessary for the system to adapt locally to the new simulation parameters. Then, equilibration runs are performed. Here, we check some thermodynamic standard properties (such as pressure or density) of the system. We

run the simulation until these properties are stabilized or the maximum number of equilibration runs is exceeded. In the latter case, the setup will be abandoned. Otherwise, the production run is started. Run lengths of $\approx 5 \cdot 10^5$ integration steps after equilibration turned out to be sufficient to determine smooth RDFs. The two examples treated in the following are at different densities: the PVA is in the dense melt, whereas the PAA is considered in very dilute solution.

III. COARSE GRAINING OF POLYMER OLIGOMERS

A. Poly (vinyl alcohol) oligomers

The coarse graining of PVA is based on all-atom simulations with the force field published in Ref. 17 using the program YASP [18]. The atomistic system containing 48 atactic decamers [$\text{CH}_3\text{CHOH}(\text{CH}_2\text{CHOH})_9\text{CH}_3$] is simulated in an orthorombic box with periodic boundary conditions at constant pressure (101.3 kPa) and constant temperature ($T = 500$ K). The integration timestep is 2 fs and the coupling times of the Berendsen manostat and thermostat are 5.0 ps and 0.2 ps (respectively). At $T = 500$ K, a trajectory of 10 ns with frames every 2 ps is generated of which we use the last 5 ns for evaluation of target distributions. The average density is 1.03 kg/m^3 . Distributions of bond lengths, angles, and torsions are determined excluding the outermost methyl groups. For comparison, analysis of the PVA trajectories of Ref. 19 with the lowest water content at $T = 375$ K yields quite similar distributions.

1. Mapping and target functions

The first step of the coarse-graining procedure is to choose a center of the CG beads. As we motivated in the introduction, we want to go beyond the simple united atom model (incorporating hydrogens into their parent carbons) and choose one CG bead per chemical repeat unit, i.e. two backbone carbons. Natural choices are (i) the center of mass of the monomer or (ii) every second carbon atom on the backbone. With respect to both mapping points, the bond length and angular distributions are determined. The distributions look quite similar for both possibilities. However, for choice (ii) they are slightly sharper (not shown). Moreover, the bond length distribution is entirely independent of the angular distribution. This is very convenient, since one has not to worry about cross-correlations which would make the mapping more complicated. For this reason, we finally choose the backbone carbon of the CHOH group as the mapping point for the CG beads (see Fig. 2). As target RDF we use the distribution function where the distances between the first four neighbors along a chain are excluded. The rationale is that the non-bonded potential of a dense melt should rather reflect the interchain interaction. For the (short-range) intrachain interactions there are already the bond stretching and bending potentials to determine the right structure. Fig. 3 contains both, the RDF of all pairs as well as the target RDF where the first four neighbors along the chain are excluded. The target RDF is quite similar to typical RDF of a dense LJ-liquid.

2. Potential parameterizations

A Gaussian bell function $P(l)$ is found to represent the distribution of two successive backbone carbons of the CHOH group (not shown). It is Boltzmann-inverted to obtain V_{str} as a harmonic potential, as stated in Equation 3.1. For PVA, the bond length between neighboring CG beads is 0.26 nm with $\sigma^2 = 0.006 \text{ nm}^2$ according the choice of the mapping.

$$V_{str}(l) = kT \ln (P(l)) \quad (3.1)$$

We analyse the intrachain distributions of the atomistic trajectories in order to find suitable CG potentials. The angular distribution between three successive $C^{(2)}$ atoms is shown in Fig. 4. It exhibits 3 peaks which can be attributed to trans-trans, trans-gauche and gauche⁺-gauche⁻ states of the two dihedral angles on the atomistic backbone between the CG points. The Boltzmann-inverted angular distribution (potential of mean force, cf. Fig. 5)

$$V_{bend}(\alpha) = kT \ln (P(\alpha) / \sin \alpha) \quad (3.2)$$

is used as a first approximation of the angular potential in the CG simulations. In this case it turns out that the CG simulation yields almost the same distribution and, hence, no further optimization needs to be performed. Since the torsional distribution between four successive CG points does not show any particular structure, we run the CG simulations without a torsional potential.

The last issue of the CG force field is, thus, the non-bonded interaction which determines the excluded volume. The optimization of this non-bonded potential according to the procedure of Ref. 11 is described in the next subsection. The target RDF is quite ‘well-behaved’ with a broad first peak (Fig. 3). After the experience of Ref. 11 we need a potential which is softer than a simple Lennard-Jones (LJ) type potential and we start with the following general ansatz:

$$V_{vdw}(r) = \frac{a_6}{r^6} + \frac{a_8}{r^8} + \frac{a_9}{r^9} + \frac{a_{10}}{r^{10}} + \frac{a_{12}}{r^{12}} \quad (3.3)$$

Note that it is switched off for directly linked CG beads as well as for next nearest neighbours in order to separate its influence from the bond angle potential.

3. Optimization procedure

The volume is fixed to obtain the correct density, whilst the non-bonded potential is varied until the RDF of the corresponding atomistic distribution is well reproduced. The merit function which is minimized is a least squares difference between the RDF $g_{CG}(r)$ of the CG system and the atomistic target RDF $g_t(r)$ integrated over a certain range:

$$f_{rdf} = \int_{r_{min}}^{r_{max}} w(r) (g_t(r) - g_{CG}(r))^2 dr . \quad (3.4)$$

$w(r) = \exp(-r)$ is a weighting function which additionally penalizes deviations at small separation. [11] Practically, the integration is performed as a sum with stepsize $dr = 0.0052$ nm.

As the target RDF of PVA is similar to the RDF of dense LJ-liquids, we started with a LJ6-9 potential as a first approximation:

$$V(r) = -\varepsilon \left(\left(\frac{\sigma}{r} \right)^6 - \left(\frac{\sigma}{r} \right)^9 \right) . \quad (3.5)$$

The LJ-type parameters ε and σ are optimized with a two-dimensional simplex. The cutoff radius for the CG-simulation is 1.1 nm (the same as in the atomistic simulations) as well as the cutoff for integration in the merit function. The best trial RDF we find within 20 steps is shown in Fig. 3. The corresponding potential parameters are $\varepsilon = 0.5$ kT/mol and $\sigma = 0.53$ nm. The slope of the first peak is still too high. We expect no significant improvement with the potential of Equation 3.5. This is because the ascent of the main peak has a smaller slope than it may be reproduced by the LJ6-9 potential with, *at the same time as*, the second peak still fitting.

Next, potential (3.3) is used with all even powers in the following parametrization:

$$V(r) = -\frac{\varepsilon}{r^{12}} \left(r^6 - 0.75 (\mu_1^2 + \mu_2^2 + \mu_3^2) r^4 + 0.6 (\mu_1^2 \mu_2^2 + \mu_2^2 \mu_3^2 + \mu_1^2 \mu_3^2) r^2 - \nu \mu_1^2 \mu_2^2 \mu_3^2 \right) , \quad (3.6)$$

where ε is a global scaling factor, μ_i are the locations of the extrema and ν is a sort of smoothing parameter (this potential is derived in the appendix of Ref. 11). A 4-dimensional simplex is used with ε , $\mu_1^2 = \mu_2^2$, μ_3^2 , and ν as variables. With ν slightly above 0.5 this yields a potential which resembles a LJ-type function, however, the minimum being much broader. After guessing some start values for this parametrization, the simplex algorithm was stopped after 32 steps. The best result was quite similar to that shown in Fig. 6.

However, with respect to future applications that will involve constant-pressure simulations, we are not satisfied just reproducing the RDF, but we would like to have the excluded volume in equilibrium with the experimental density. This means we are searching for a potential yielding a pressure near zero. For this, we modify the merit function of the simplex algorithm to include a term measuring the deviation of the pressure from zero:

$$f_{\text{tot}} = f_{\text{rdf}} + w_p (p - p_0)^2 , \quad (3.7)$$

with the target pressure $p_0 = 0.1$ (LJ units) and a relative weight $w_p = 0.2$. This gives still a rather small weight to the pressure to permit sufficient fluctuations for testing the parameter space. The evolution of the pressure and the merit function is shown in Fig. 7). The algorithm converges to a minimum of the merit function which represents a satisfying result. The best value is already obtained in step 21 and is the one shown in Fig. 6. The corresponding parameters are $\varepsilon = 12$ kT, $\mu_1 = 0.41$ nm, $\mu_3 = 0.58$ nm, and $\nu = 0.517$. Fig. 6 contains also the potential scaled by a factor of 10 to show its two repulsive regimes: a really excluded hard shell below 0.4 nm and a softer core above this value to the minimum at 0.59 nm.

B. Poly (acrylic acid) oligomers

For PAA, the optimization is based on atomistic simulation data (also generated using the YASP package) by Biermann and Müller-Plathe [20]. They studied one fully deprotonated, atactic oligomer strand of 23 monomers in 3684 water molecules at ambient conditions. Sodium counterions were included to achieve overall charge neutrality. The total simulated time was 9 ns. We map this system to the mesoscale by replacing one repeating unit (i.e. one monomer) by one bead. Additionally, the water solvent is removed as shown in Fig. 1. The simulated CG system contained 460 particles (20 23-mers, for technical reasons) at density $\rho = 0.1962\sigma^{-3}$. This density is adapted from the atomistic simulation and corresponds to the highly diluted regime. The chains do practically not interact with each other. Moreover, one must be aware of the problem that we are dealing with a highly charged polymer. One might think, that the long-range character of the Coulomb interactions does not allow for them to be neglected in the CG model. In our case this is not correct for two reasons: First and most importantly, the Debye length (characterizing the relative importance of the electrostatic energy compared to thermal energy) of the system is close to the Debye length of water, which is 0.7 nm. This corresponds approximately to the distance of two non-bonded CG monomers. Hence, the Coulomb interactions can be neglected for larger distances to a good approximation. Second, the atomistic simulations were (for sake of the first reason) performed with a reaction field approximation of the Coulomb interactions, implying that already the atomistic simulation does technically not include any long-ranged interaction. Note finally, that for short distances charges will still be present implicitly in the CG force field. They are, as the PAA-solvent interactions, reflected in the intrachain RDF and in the CG potential resulting from it.

1. Mapping and target functions

Again, the first question is how to define the coarse-grained beads. Exactly as in the case of PVA, we want to incorporate an essential amount of atomistic information in our coarse-grained model. For PAA, three choices seem to be appealing, cf. Fig. 8. Either, we could choose the backbone carbon which is linked to the side group (marked 1 in Fig. 8) or the side-group carbon (2) or the center of mass of a $(-\text{CH}(-\text{COOH})-\text{CH}_2)$ repeating unit (3). To make a decision, we revisited the atomistic trajectory and investigated the intrachain distance and angular distributions for these candidates. They are presented in Fig. 9. For the distance distribution (Fig. 9a), the sharpest peak originates from the backbone CH carbon atom [possibility 1]. This is understandable because adjacent CH carbons are directly linked via two covalent bonds, leaving not much configurational freedom. In contrary, the sidegroup has rotational freedom to move such that the distribution of the COO^- carbon [possibility 3] is much broader around a much larger mean value. The center of mass of a repeat unit [possibility 2] lies somewhere in between. For the angular distributions, the first observation is that side group (3) and backbone carbon (1) distributions have very different peaks. In view of this, the behaviour of the center-of-mass distribution made us choose it for the mapping: it has a reasonably sharp distance peak and the angular distribution includes some

of the behaviour of the side group. So, it represents a compromise between our preference for sharp peaks and the need of taking into account the side group.

Now that we determined the mapping, we need a meaningful target function. In contrast to PVA, exclusively intrachain properties can be chosen because Biermanns simulation contained only one polymer strand in solution. Analysis of the various atomistic intrachain radial distribution function (RDF, RDF-a and RDF-b, Section IIA) reveals that the full RDF can be decomposed (Fig. 10). The first peak originates exclusively from the nearest neighbours as it would be the only one which remains when taking the difference between full RDF and RDF-a. So, this peak is determined by the distance distribution of adjacent center-of-mass points. Similarly, the next two peaks are mainly resulting from the second-nearest neighbours. They correspond exactly to the peaks of the angular distribution, as shown in Fig. 9 and, hence, are dominated by this distribution. After that, non-bonded interactions start to influence in the RDF.

For the optimization procedure (and the target function(s)), it has the following consequences: as we stated in Section IIA the relative strength of the various potential terms should be taken into account. The strongest one is the bond stretching potential V_{str} . Since the corresponding peak is the overall sharpest and almost normally distributed, we skip any optimization in favour of a reduction of parameters. Instead, we approximate the atomistic center-of-mass distance distribution by a Gaussian function $P(l)$ and Boltzmann-invert it to obtain $V_{str}(l)$ (cf. Equation 3.1). On the other side, the weakest potential we could take into account is the torsional potential. Although the distribution (not shown) is not flat as in the case of PVA, the question arises whether it is too unimportant to make any significant contribution to the outer peaks in the RDF or not. In a first optimization process, we therefore decided to not include it in the coarse-grained force field at all. We discuss this point in more detail below (Section IIIB4).

So for the moment, we are left with the bond-bending potential V_{bend} and the non-bonded potential V_{vdw} . The optimization of these can be split up into three parts: First, V_{bend} will have its strongest influence on the following two peaks and is, hence, optimized against the RDF-a. Second, the non-bonded potential has to be optimized. In order to separate its influence on the RDF-a main peaks, we switch V_{vdw} off for 1-2 and 1-3 interactions. It is then optimized against the RDF-b. It makes no sense to choose the full RDF or RDF-a for this optimization because they are dominated by the 1-2 and 1-3 interactions, while the RDF-b reflects only 1-4 and higher interactions. Third, the best parameters from the separate optimizations are taken as start values for a mixed optimization against the RDF-a which responds strongest to variations of both the bond bending and non-bonded potential.

2. Potential parameterizations

For the CG bond stretching potential, the atomistic output distribution of two successive center-of-mass monomers is investigated. The mean value of the Gaussian $P(l)$ is determined to be 0.363 nm and the standard deviation is 0.022 nm. These values are neither changed nor optimized in the CG model, as stated in Section IIIB1, but transformed into a potential energy according to Equation 3.1. The atomistic output distribution for the center-of-mass

angles can be approximated well by two Gaussians, as shown in Fig. 11. In contrast to the PVA model, we do not convert *this* distribution into a potential function. Instead, we use an auxiliary distribution which, transformed, gives the CG bending angle potential. It has the same qualitative shape but differs in details. The approximation provides us with four parameters for the CG optimization: relative peak height, relative peak position and the two standard deviations. The values of the fit are given in Table I. The standard deviations of the two peaks are very similar. In order to lower the number of parameters, we sometimes freeze their ratio and constrain them to their atomistic value of $\sigma_1^G/\sigma_2^G = 0.92$. Varying the Gaussian parameters, we can generate physically understandable new bond angle distributions. They are transformed into CG bond angle potentials V_{bend} , by application of Equation 3.2.

For the non-bonded interactions, we perform simulations using a standard LJ6-12 potential with ε and σ as test potential to get a feeling for the excluded volume behaviour of the chains, i.e. $V(r)$ of Equation (3.8) is applied.

$$V_{\text{LJ6-12}}(r) = 4\varepsilon \left(\left(\frac{\sigma}{r} \right)^{12} - \left(\frac{\sigma}{r} \right)^6 \right), \quad (3.8)$$

A cutoff distance of 2.52 nm is imposed for this potential. As for PVA, it is switched off for directly linked CG beads as well as for next nearest neighbours. Meaningful values for the LJ parameter are $\varepsilon = 0.384$ kT/mol and $\sigma = 0.74$ nm (no data shown). However, the LJ potential is too inflexible to cope with the demands of a suitable non-bonded potential for PAA. In particular, it does not reproduce the correct rise and peak broadness of the target RDF(s). So, we need a specially designed non-bonded potential to succeed in our optimization task:

$$V_{vdw}(r) = \begin{cases} \varepsilon_1 \left(\left(\frac{\sigma_1}{r} \right)^8 - \left(\frac{\sigma_1}{r} \right)^6 \right) & r < \sigma_1 \\ \varepsilon_2 \left(\sin \frac{(\sigma_1 - r)\pi}{(\sigma_2 - \sigma_1)2} \right) & \sigma_1 \leq r < \sigma_2 \\ \varepsilon_3 \left(\cos \frac{(r - \sigma_2)\pi}{\sigma_3 - \sigma_2} - 1 \right) - \varepsilon_2 & \sigma_2 \leq r < \sigma_3 \\ \varepsilon_4 \left(-\cos \frac{(r - \sigma_3)\pi}{\sigma_4 - \sigma_3} - 1 \right) - \varepsilon_2 & \sigma_3 \leq r < \sigma_4 \equiv r_{\text{cut}} \end{cases} \quad (3.9)$$

This potential was previously applied to tetrahydrofuran (THF) and diphenyl carbonate (DPC). [11] It consists of a hard core repulsion, using a LJ6-8 potential. This means it is weaker than a standard LJ6-12 which is useful for CG simulations because center-of-mass points can approach each other more closely than atomic cores for which the original LJ6-12 was designed. However, a strictly forbidden excluded volume region remains. The next two parts are also repulsive, with force minima at σ_2 and σ_3 . This enables us to generate an RDF with a first peak or a shoulder at σ_2 and a second one above σ_3 . These features are essential, as we will see in the next section.

3. Optimization procedure

The simplex optimization was discussed in full detail in foregoing publications. [10,11] Therefore, we will only state our start simplices and final results.

During the first stage, we optimize the CG bond angles against the RDF-a. The non-bonded interactions are held fixed and simulated with some few test guesses for the LJ6-12 potential ($\epsilon = 0.2 - 1.75$ kT/mol and $\sigma = 0.65 - 0.8$ nm). As stated in the previous subsection, they are not switched on before the 1-4 distance between the beads. We, therefore, do not expect them to have much influence on the 1-3 peaks which dominate the RDF-a. Therefore, non-bonded test guesses are sufficient at this stage of the simplex optimization. As start simplex of a typical simulation at this stage, we use e.g.:

#	eps	sig	amp1/amp2	std1	merit function f_a
#1	0.384	0.74	1.95	5.0	234.644
#2	0.384	0.74	2.20	6.5	188.777
#3	0.384	0.74	1.90	7.5	251.345
#4	0.384	0.74	1.95	8.0	255.425
#5	0.384	0.74	2.50	9.0	208.890

Fig. 12 shows some results obtained during the course of the optimization process. The relative amplitudes and the standard deviation of the distribution of the first peak are used as optimization variables (Fig. 12a). The standard deviation of the other peak is adjusted as described in Section IIIB 2. A qualitative match of the CG peaks and the atomistic peaks can be observed for the resulting RDF-a (Fig. 12b). Still, the height of the main peaks is not sufficiently well reproduced and for too low a standard deviation ($< 6^\circ$), an unwanted dip appears between the main peaks (at $r \approx 0.6$ nm). It turns out that it is favourable for the simplex to overshoot the intensity of the 90 degree peak by 15 – 30% and to sharpen the peaks by a considerable amount of 30 – 50% compared to the atomistic initial distribution. This follows from the fact, that the weight function decays exponentially. Therefore, inner peaks are tried to be matched first. For the sharpening of the CG input distribution, however, there is also a physical reason: the target pair distribution functions we observe in the atomistic simulations is the Boltzmann-inverse of a potential of mean force (at finite temperature). Hence, it is less sharp than the CG distribution which is the Boltzmann-inverse of a potential energy at $T = 0$ K.

After some series of simulations it became clear, that the details could not be optimized by varying the bond angle parameters only. The relative width of both standard deviations need not be systematically modified with respect to the atomistic case. The same holds for the position of the main peak. This leaves us with three parameters for post-optimization at stage three: side peak position, relative peak height and one standard deviation.

Therefore, we fix an intermediate set and turn to stage two, the non-bonded parameter optimization against the RDF-b. Typical examples of the results are presented in Fig. 13. Clearly, the LJ6-12 optimization is rather unsuccessful (cf. Fig. 13(a)). Only one of either the rise of the pre-peak or the rise of the main peak can be matched. The descent does not show at all the characteristic structure of the target function from the atomistic simulations. Therefore, we need to move over to a potential which is tailored to the following requirements: (i) a repulsive core to suppress too close contacts and to mimic the sharp rise of the pre-peak correctly. (ii) a tiny plateau to determine the width of the pre-peak. (iii) a second softer repulsive region to grasp the ascent of the main peak and (iv) an attractive tail to adequately reproduce the main peak descent. (As it turns out, a well-shaped main peak of the RDF-b

will be followed by acceptable side peaks.) The potential V_{vdw} given in Equation 3.9 fulfills all these demands.

Test runs with this modified potential are already much better compared to the LJ6-12 potential. However, V_{vdw} consists of eight parameters. This makes it difficult to optimize all of them at the same time for two reasons. First, the computational demand gets quite high. Second, and more importantly, such a simplex will be trapped more easily in a local minimum, if one cannot guess at least some of the parameters well. If this high-dimensional space is dominated by one or two of the eight parameters (a very frequent case from our experience, cf. Ref. 11), the merit function will not change much if some weak parameters are driven in the wrong direction of a local minimum. Hence, we only choose three to five parameters for one optimization series and fix part of them for a subsequent series in favour of optimizing another subset. Fig. 13(b) shows two examples of a simplex started with:

#	sig1	sig2	eps2	eps3	eps4	merit function f_b
#1	0.505	0.065	0.5	2.5	0.3	44.1712
#2	0.510	0.065	0.6	2.0	0.4	17.8984
#3	0.520	0.053	0.4	2.3	0.5	23.8493
#4	0.505	0.060	0.5	2.1	0.5	19.0945
#5	0.505	0.068	0.6	2.4	0.4	34.4716
#6	0.510	0.060	0.4	2.2	0.6	24.4090

Here, we fix the pre-optimized non-bonded parameters $\varepsilon_1 = 14.0$ kT/mol, $\sigma_3 = 0.79$ nm and $\sigma_4 = 1.3$ nm. In the case of σ_3 , this is physically motivated: it corresponds to the potential minimum and matches the main peak position of the RDF-b, for σ_4 the value is almost arbitrarily chosen in the vicinity of values for which the LJ6-12 test potential decayed to $0.01 \cdot \varepsilon_{LJ}$. As best fit (shown in Fig. 13), this simplex yields

```
#19      0.505137 0.073784 0.750695 1.512260 0.314712 10.9107
```

It turns out that some parameters could be determined easily and precisely individually while the interplay of others generates strong oscillations in the merit function f . Those are $\varepsilon_2 - \varepsilon_4$ because they massively influence the probabilities of the closest approach of the CG beads, i.e. determine the relative strength of the peaks. Consequently, they are taken to be post-optimized in the third stage together with the crucial bond bending parameters.

Some of the simplex points encountered during the final optimization runs are the following:

#	amp1/amp2	peak2	std1	eps2	eps3	eps4	merit f_a
#2	1.9	(118.2)	(6.8)	0.700000	2.300000	0.350000	83.2977
#7	2.088	(118.2)	(6.8)	0.430000	2.548000	0.540000	50.2795
#8	1.983	(118.2)	(6.8)	0.372000	1.847200	0.566000	85.8116
.							
.							
#13	(1.90)	(118.2)	(6.8)	0.387200	2.304243	0.522016	48.9554
.							
.							

#7	(1.90)	117.031	6.743750	(0.39)	(2.31)	0.437500	47.1609
#24	(1.90)	116.060	6.716646	(0.39)	(2.31)	0.428761	41.0346
#33	(1.90)	116.555	6.769754	(0.39)	(2.31)	0.463141	39.4119
#42	(1.90)	116.709	6.768629	(0.39)	(2.31)	0.463242	37.843

Numbers in brackets denote parameters which are not optimized in the corresponding run. Although this is just a small selection from the optimization, the points demonstrate the relative strength of the parameters. The first line contains (as it turns out) three almost optimized parameters, but the wrong relative strength of ε_2 and ε_4 destroys a good value of f . The latter is the overall most dominant parameter in this line. The final result is listed in Table I (bonded parameters) and Table II (non-bonded parameters). It is visualized for all RDFs in Fig. 14. All functions are reproduced qualitatively correct. For such a complicated molecule like PAA, this is all we could expect for a first trial.

4. An improved model

A first test is the torsional output distribution of the CG simulations, i.e. the first intramolecular degree of freedom not already accounted for by a force field term. The final force field generates a qualitative agreement for the torsions, as shown in Fig. 15. The solid line represents the atomistic output distribution, the line with the circles the CG distribution. Still, the details of the original distributions can not be reproduced. Also the difference between the peak and the valley is too large. More importantly, we encounter the following problem when we tried to apply the CG force field to long polymer chains: for our test chain length of 460 repeating units, we observe a collapse of the chain. It originates from the deep attractive part of V_{vdw} . Interestingly, that happens although the radius of gyration coincides well with the atomistic one for chain length 23 (cf. Table III) and although artificial 23-subchain RDFs of the 460-mer (which corresponds to a PAA sample with 43250 g/mol) almost coincide with the original CG one (data not shown). Due to this observations, we decide to introduce torsions to the CG force field in order to redistribute some degrees of freedom in a way that the attractive part of V_{vdw} can be lowered. Therefore, the following corrections are applied: first, the depth of the attractive tail characterized by ε_4 is lowered by one order of magnitude and, second, the atomistic torsional output distribution (cf. Fig. 15) is used as additional input potential in the CG picture. The optimization has to be corrected accordingly. Tests show at once, that torsions have a strong influence on the RDF-b. Figure 16 shows an RDF with a fully optimized potential compared to runs with some interaction switched off. Without a non-bonded potential, the ascent of the main peak starts at too small distances. That means that the torsional potential is not strong enough to straighten the chain sufficiently. Still, the pre-peak is better reproduced than in the full optimization case. If, conversely, the torsional potential is taken away, the pre-peak is even better reproduced. This shows, that also the torsions help to straighten the chain. Additionally, they make the main peak more pronounced which can be deduced from the broadened descent without them. Most importantly, they are capable of correcting the long-chain structure. Re-runs of the 460-mer prove that the CG PAA behaves like a chain in a good solvent. We find a hydrodynamic radius of $R_H = 5.31 \pm 0.26$ nm for this system, which compares rather

well with an experimental value of $R_H = 5.27 \pm 0.60$ nm for a PAA sample of 36900 g/mol (corresponding to a 393-mer).

IV. DISCUSSION AND CONCLUSIONS

This work demonstrates the extension of the methods developed in Ref. [11] to polymers where bonded as well as non-bonded interaction parameters have to be determined. The simplex optimization method works also for oligomers under very different conditions with respect to density and charge state. In the dense melt one has to increase the equilibration times with respect to the simple liquids of Ref. [11]. For poly (vinyl alcohol), it was also shown how to optimize structural and thermodynamic quantities at the same time. Including the pressure in the merit function has led to a coarse grained potential with attractive as well as repulsive interactions. Therefore, the force field can be used in constant-pressure simulations or to model e.g. surfaces. The Boltzmann-inverted angular distribution was, in combination with the development of a specific non-bonded potential, sufficient to reproduce the target function(s). For poly (acrylic acid), the situation is more complicated. Here, several important conclusions can be drawn. First of all, we proved that the simplex algorithm is also capable of optimizing bonded potential variables. For this purpose, partial RDFs were utilized. Their peaks could be assigned to interactions between specific intramolecular monomers which were separately optimized. The torsional potential was especially important to generate the correct long-chain behaviour. That is, because it allowed a successful non-bonded optimization with a fairly weak attractive part compared to the force field derived without it. Comparison with experimental data delivered very promising results for the hydrodynamic radius as a first test property.

This work will be continued. The simplex optimization is a very effective tool for generating reliable coarse-grained force fields if one adds human intuition to create meaningful start guesses. Special non-bonded spherical potentials turned out to be very useful to resolve double peaks, without having to resort to complicated ellipsoidal potentials. The speed-up of the simulated time compared to atomistic simulations is enormous. This will make it possible to study properties of polymers which are entropically dominated and which are far too long-ranged to be treated by brute-force atomistic simulation. At the same time, the parameterization procedure ensures that enough of the chemical identity of the polymer is kept to allow investigations and deeper understanding of specific systems. The PVA force field is intended to be used for equilibrating large samples with surfaces. The PAA force field shall be utilized to simulate several long PAA strands. That will indicate the transferability of the model and a thorough test against experiments.

After completing this paper we learned about some interesting related work [21]. The authors proceed according to the same idea of optimizing the interactions of coarse-grained polymer models with respect to structural properties. However, their method and aim are quite different: Using a Monte Carlo sampling method they optimize interaction parameters on a much coarser level of blobs representing larger subchains. While this might be useful for melt simulations, their procedure abandons too much details for our interest in surface properties.

ACKNOWLEDGEMENTS

We would like to thank Beate Müller and Simone Wiegand for experimental PAA measurements of the hydrodynamic radius. Oliver Biermann is acknowledged for making available his atomistic PAA data as well as for technical improvements of the simplex optimization and Oliver Hahn for contributing an MD program for chains of spherical particles.

REFERENCES

- ¹ J. Baschnagel, K. Binder, P. Doruker, A. A. Gusev, O. Hahn, K. Kremer, W. L. Mattice, F. Müller-Plathe, M. Murat, W. Paul, S. Santos, U. W. Suter and V. Tries, *Adv. Polym. Sci.* **152**, 41 (2000).
- ² B. Forrest and U. W. Suter, *J. Chem. Phys.* **102**, 7256 (1995).
- ³ I. Carmesin and K. Kremer, *Macromolecules* **21**, 2819 (1988).
- ⁴ W. Paul, K. Binder, K. Kremer, and D. Heermann, *Macromolecules* **24**, 6332 (1991).
- ⁵ J. Baschnagel, K. Binder, W. Paul, M. Laso, U. W. Suter, I. Batoulis, W. Jilge and T. Bürger, *J. Chem. Phys.* **95**, 6014 (1991).
- ⁶ P. Doruker and W. Mattice, *Macromolecules* **30**, 5520 (1997).
- ⁷ P. Doruker and W. Mattice, *J. Phys. Chem. B.* **103**, 178 (1999).
- ⁸ R. Groot and P. Warren, *J. Chem. Phys.* **107**, 4423 (1997).
- ⁹ P. Espanol, M. Serrano, and I. Zuniga, *J. Mod. Phys. C* **8**, 899 (1997).
- ¹⁰ R. Faller, H. Schmitz, O. Biermann, and F. Müller-Plathe, *J. Comput. Chem.* **20**, 1009 (1999).
- ¹¹ H. Meyer, O. Biermann, R. Faller, D. Reith, and F. Müller-Plathe, *J. Chem. Phys.* accepted (2000).
- ¹² W. Tschöp, K. Kremer, J. Batoulis, T. Bürger, and O. Hahn, *Acta Polymer* **49**, 61 (1998).
- ¹³ W. Tschöp, K. Kremer, O. Hahn, J. Batoulis, and T. Bürger, *Acta Polymer* **49**, 75 (1998).
- ¹⁴ J. Eilhard, A. Zirkel, W. Tschöp, O. Hahn, K. Kremer, O. Scharpf, D. Richter and U. Buchenau, *J. Chem. Phys.* **110**, 1819 (1999).
- ¹⁵ M. Allen and D. Tildesley, *Computer Simulation of Liquids*, Oxford Science, Oxford, 1987.
- ¹⁶ G. Grest and K. Kremer, *Phys. Rev. A* **33**, 3628 (1986).
- ¹⁷ F. Müller-Plathe and W. F. van Gunsteren, *Polymer* **38**, 2259 (1997).
- ¹⁸ F. Müller-Plathe, *Comp. Phys. Comm.* **78**, 77 (1993).
- ¹⁹ F. Müller-Plathe, *J. Membrane Sci.* **141**, 147 (1998).
- ²⁰ O. Biermann and F. Müller-Plathe, in preparation (2000).
- ²¹ R. L. C. Akkermans, *A structure-based coarse-grained model for polymer melts*, PhD thesis, University of Twente (Netherlands), 2000, chapter 5.

TABLE I. Fit results (of two Gaussians to the data) for the atomistic bending angle distribution as well as optimized parameters for the CG model of the PAA center-of-mass repeat unit [possibility 2].

Peak #	position [$^{\circ}$]	standard deviation [$^{\circ}$]	peak height [height of peak 2]
Atomistic fit results			
1	88.5	10.7	1.72
2	118.2	11.6	1.00
force field without torsional potential			
1	88.5	6.8	1.90
2	116.7	7.4	1.00
force field including torsional potential			
1	88.0	6.8	1.72
2	116.7	7.4	1.00

TABLE II. Optimized non-bonded parameters for the coarse grained PAA simulations.

	σ_1	ε_1	σ_2	ε_2	σ_3	ε_3	$\sigma_4 = r_{cut}$	ε_4
force field without torsional potential	0.507	11.3	0.569	0.390	0.790	2.31	1.3	0.50
force field including torsional potential	0.496	11.3	0.559	0.353	0.775	0.49	1.3	0.05

TABLE III. Radius of Gyration [nm] for PAA 23-mers. Comparison between atomistic and coarse grained chain.

$R_G^{atomistic}$	R_G^{CG} without torsions	R_G^{CG} including torsions
1.28 ± 0.08	1.24 ± 0.05	1.25 ± 0.05

List of Figures

1	Mapping from atomistic model to mesoscale model. The atomistic model comprises one poly (acrylic acid) (PAA) 23-mer, water and counterions to achieve charge neutrality. The PAA chain with one bead per atomistic monomer is the only component reappearing after the mapping.	22
2	Illustration of the mapping of the atomistic PVA oligomer to a coarse-grained bead-spring model. One bead represents one chemical repeat unit, a spring spans two carbon-carbon bonds on the backbone. The angle between three CG beads results from two successive atomistic torsions.	23
3	Model PVA monomers with a LJ6-9 potential. Thick continuous line: target distribution from atomistic simulations with 10mers (RDF between all monomers excluding the 4 nearest neighbors on each chain), thin line: RDF between all monomers from atomistic simulations (the sharp peaks at 0.26 nm and 0.52 nm are due to the first and second nearest neighbors on the chains). Squares: RDF of CG simulation with LJ6-9 potential. Best RDF out of 20 simplex steps.	24
4	Histogram of angles between successive coarse-graining points (every second backbone carbon) for PVA obtained from the atomistic simulation.	24
5	Potential of mean force of the CG-angle distribution for PVA.	25
6	Model PVA monomers with a 6-8-10-12 potential. Thick continuous line: target distribution from atomistic simulations with 10mers (RDF between all monomers excluding the 4 nearest neighbors on each chain). Squares: RDF of CG simulation with the 6-8-10-12 potential. The corresponding potential is also plotted.	25
7	Evolution of the pressure (circles) and the merit functions (squares) during one simplex optimization run for PVA 10mers. Open squares show the merit function f_{rdf} of the deviation from the target RDF. The filled squares represent the total merit function according to equation (3.7.)	26
8	Various possibilities how to define the sphere center of the coarse grained beads for PAA. Assuming that one bead should correspond to one repeating unit (-CH(-COOH)-CH ₂), there are three obvious choices: (1) the CH backbone carbon atom, (2) the center-of-mass of the repeating unit and (3) the sidegroup carbon atom.	26
9	Intrachain distance (a) and angle distributions (b) for three choices of coarse-graining points in the atomistic model of PAA, cf. Fig. 8.	27
10	Intrachain radial distribution functions of the repeating units center of mass of PAA. The first peak originates from the bond length distribution, the next two peaks from the bond angle distribution. After this the influence of the intrachain non-bonded interactions starts.	28

11	Bond angle parametrization for the PAA CG model. The atomistic data could be fitted by two Gaussians. This leaves four parameters for the coarse graining optimization: relative peak height, relative peak position and the two standard deviations.	29
12	Bond angle potential optimization against the RDF-a for PAA. (a) Input distributions. The relative amplitudes (first number) and the standard deviation (second number) of the main peak are optimized. (b) The resulting RDF-a. For the non-bonded interactions, a LJ 6-12 potential with $\varepsilon = 0.384$ and $\sigma = 0.74$ is applied.	30
13	Non-bonded potential optimization against RDF-b for PAA. Open symbols denote the potentials, filled symbols the corresponding RDFs. Small changes in the potentials manifest themselves strongly in the trial RDFs. (a) Lennard-Jones 6-12 potential of Equation 3.8 (b) Piecewise potential of Equation 3.9	31
14	Final optimization result for PAA. Thick lines: target RDFs from atomistic simulations. Triangles: first optimization force field. Squares: improved force field, including torsions. All features of the RDF are at least qualitatively well reproduced.	32
15	Normalized distribution of the dihedral angles for PAA, obtained from the simulation. The atomistic data (solid line) is symmetrized and 7-point smoothed. The coarse grained data is obtained for the force fields without (circles) and with (triangles) torsional potential. Qualitatively, they reproduce the atomistic curve but for both, the peak is overrepresented whilst the valley is underrepresented.	33
16	Interplay of torsional and non-bonded interactions for an RDF-b of PAA. Runs with partly switched off interactions can be compared to the full optimization. Without a non-bonded potential, the ascent starts at too small distances whereas without torsions, the descent is not well reproduced. . . .	34

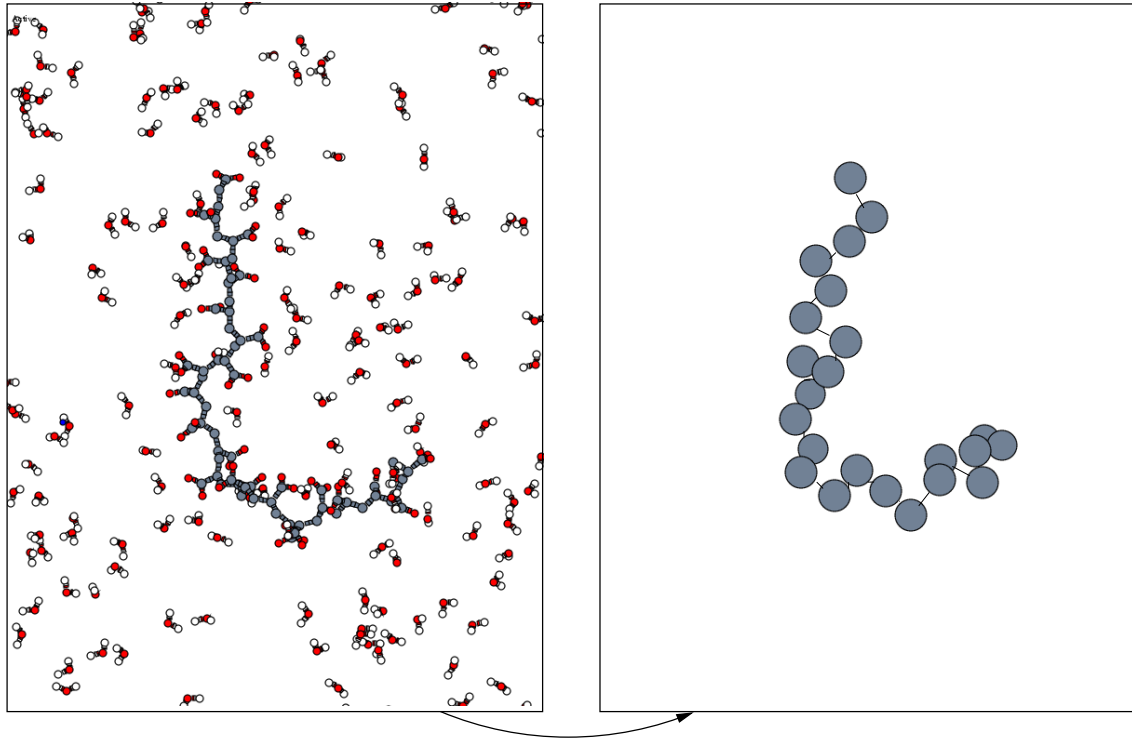


FIG. 1. Mapping from atomistic model to mesoscale model. The atomistic model comprises one poly (acrylic acid) (PAA) 23-mer, water and counterions to achieve charge neutrality. The PAA chain with one bead per atomistic monomer is the only component reappearing after the mapping.

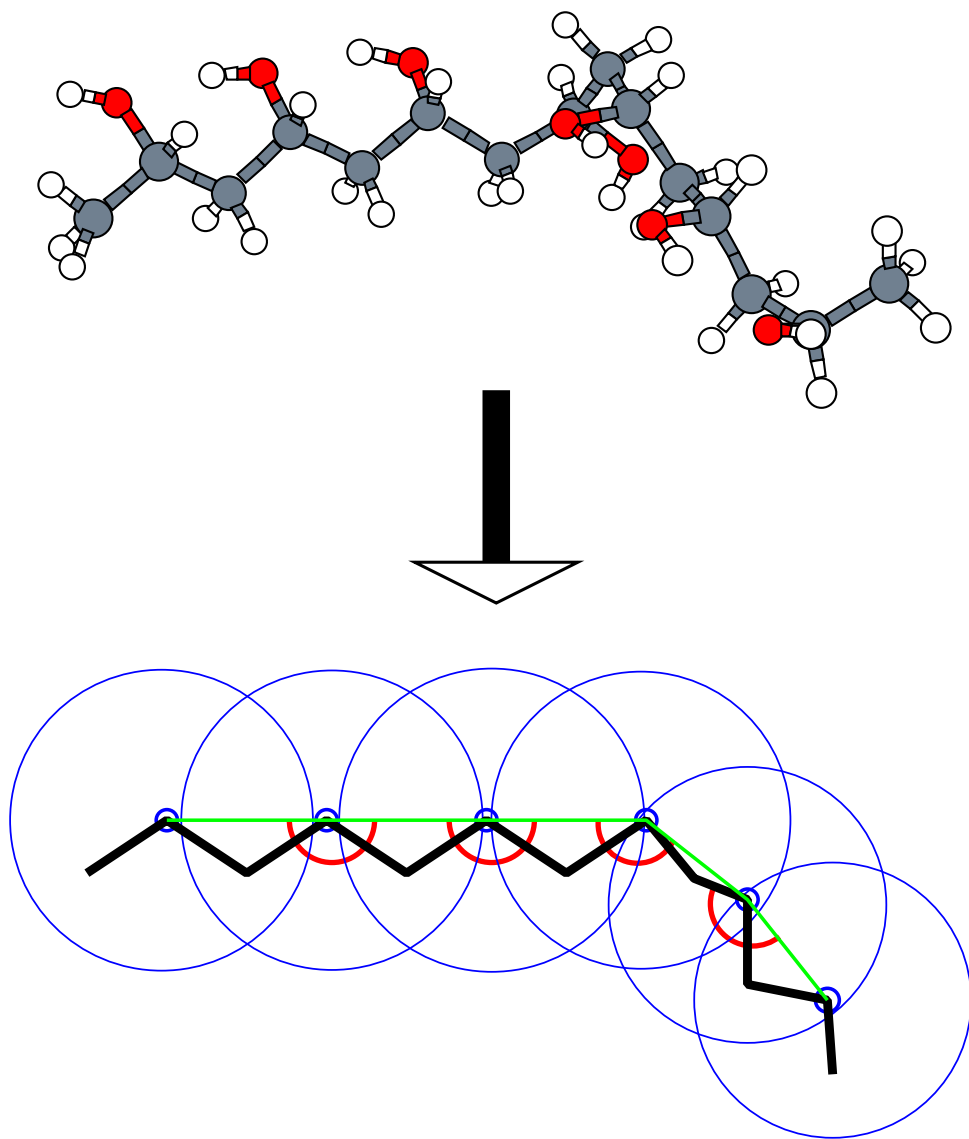


FIG. 2. Illustration of the mapping of the atomistic PVA oligomer to a coarse-grained bead-spring model. One bead represents one chemical repeat unit, a spring spans two carbon-carbon bonds on the backbone. The angle between three CG beads results from two successive atomistic torsions.

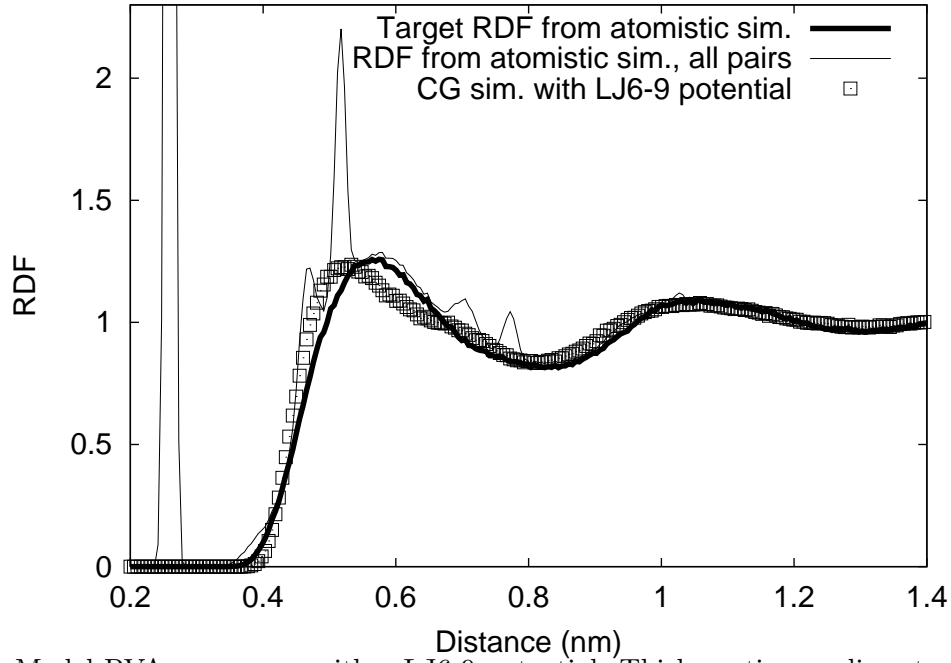


FIG. 3. Model PVA monomers with a LJ6-9 potential. Thick continuous line: target distribution from atomistic simulations with 10mers (RDF between all monomers excluding the 4 nearest neighbors on each chain), thin line: RDF between all monomers from atomistic simulations (the sharp peaks at 0.26 nm and 0.52 nm are due to the first and second nearest neighbors on the chains). Squares: RDF of CG simulation with LJ6-9 potential. Best RDF out of 20 simplex steps.

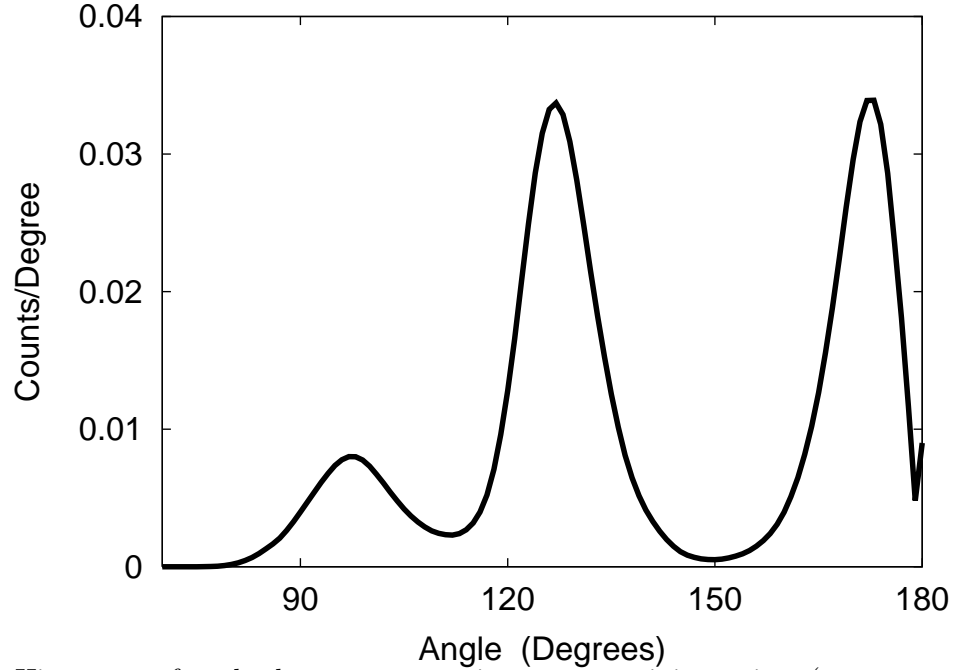


FIG. 4. Histogram of angles between successive coarse-graining points (every second backbone carbon) for PVA obtained from the atomistic simulation.

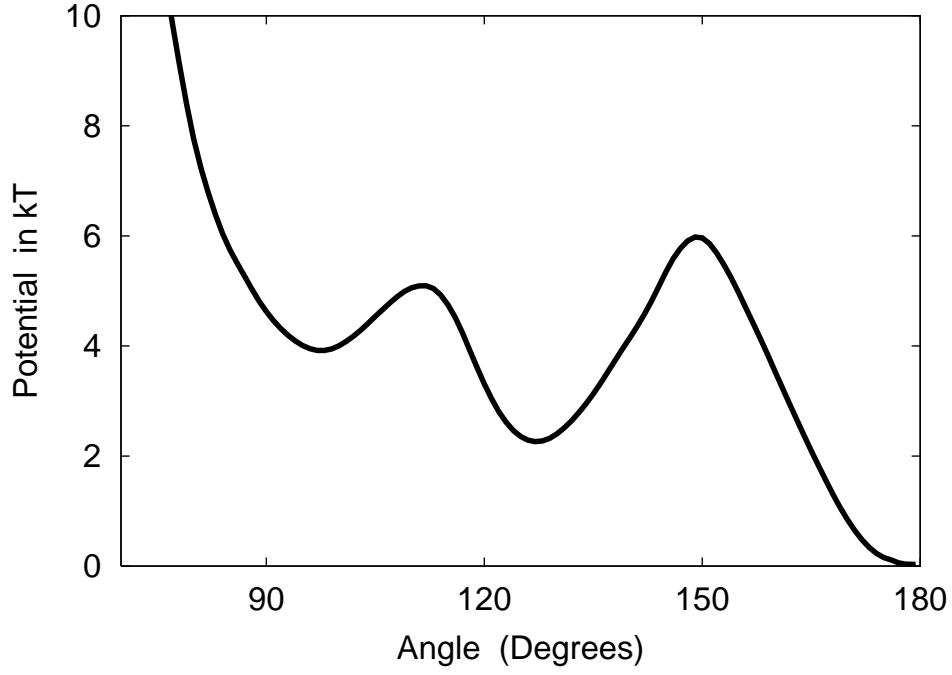


FIG. 5. Potential of mean force of the CG-angle distribution for PVA.

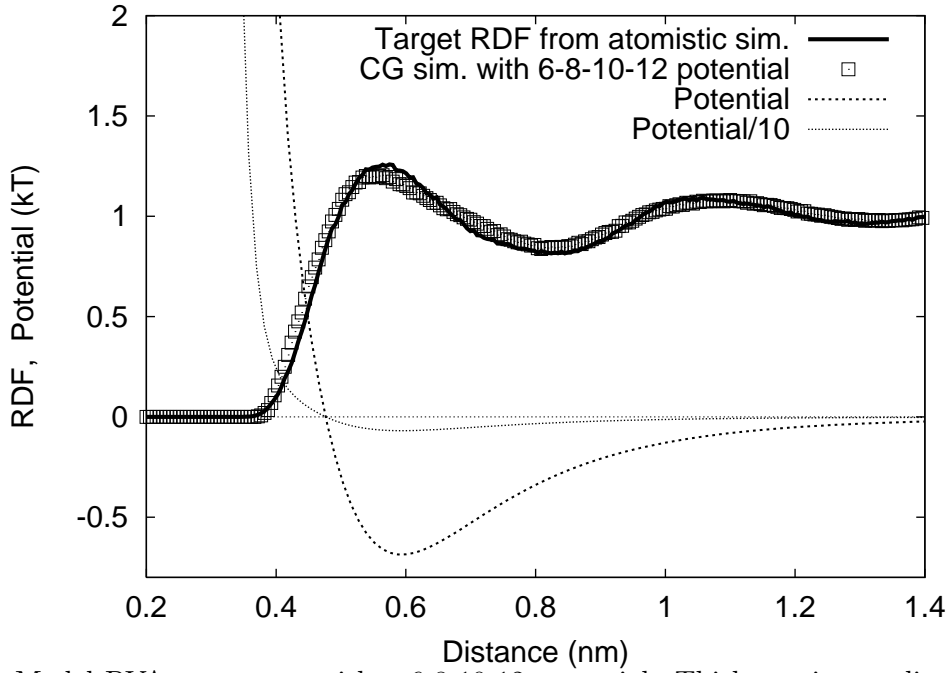


FIG. 6. Model PVA monomers with a 6-8-10-12 potential. Thick continuous line: target distribution from atomistic simulations with 10mers (RDF between all monomers excluding the 4 nearest neighbors on each chain). Squares: RDF of CG simulation with the 6-8-10-12 potential. The corresponding potential is also plotted.

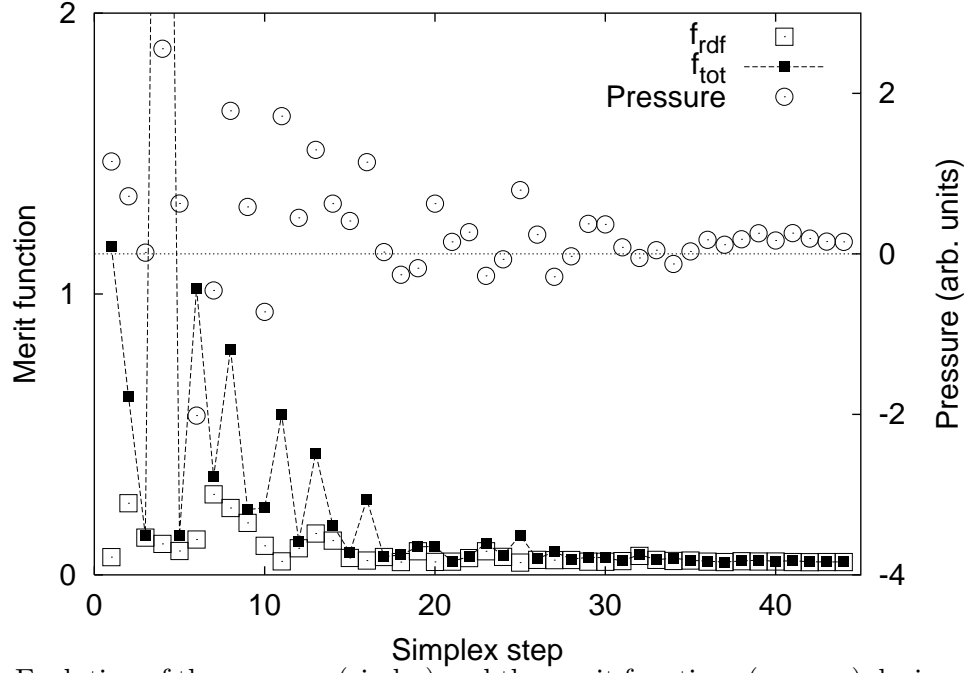


FIG. 7. Evolution of the pressure (circles) and the merit functions (squares) during one simplex optimization run for PVA 10mers. Open squares show the merit function f_{rdf} of the deviation from the target RDF. The filled squares represent the total merit function according to equation (3.7.)

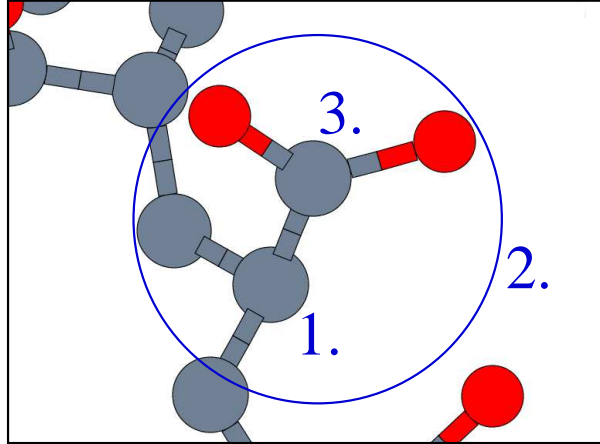


FIG. 8. Various possibilities how to define the sphere center of the coarse grained beads for PAA. Assuming that one bead should correspond to one repeating unit $(-\text{CH}(-\text{COOH})-\text{CH}_2)$, there are three obvious choices: (1) the CH backbone carbon atom, (2) the center-of-mass of the repeating unit and (3) the sidegroup carbon atom.

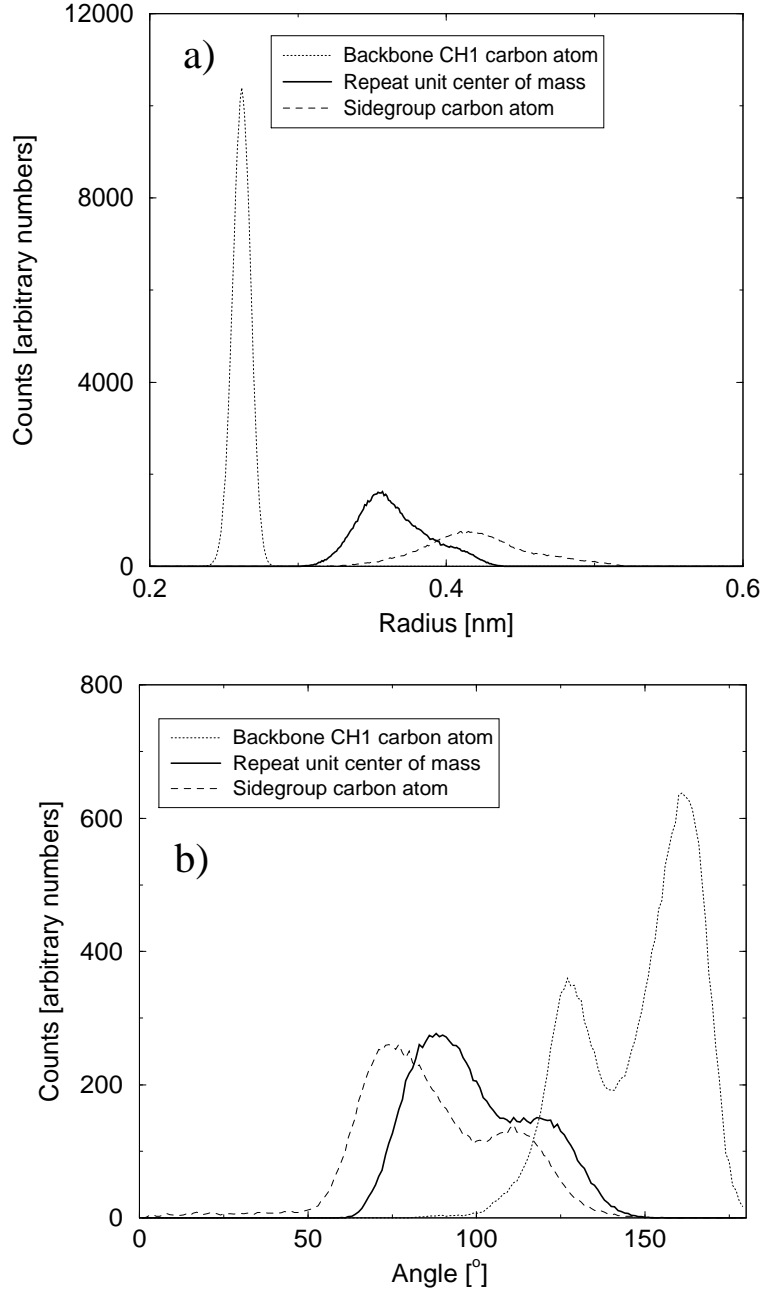


FIG. 9. Intrachain distance (a) and angle distributions (b) for three choices of coarse-graining points in the atomistic model of PAA, cf. Fig. 8.

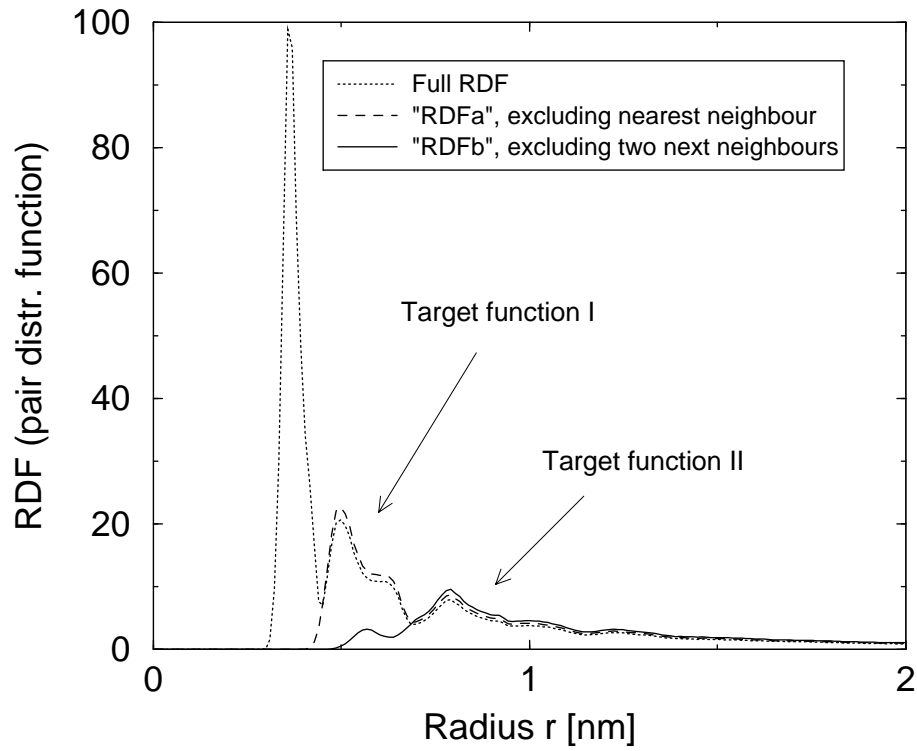


FIG. 10. Intrachain radial distribution functions of the repeating units center of mass of PAA. The first peak originates from the bond length distribution, the next two peaks from the bond angle distribution. After this the influence of the intrachain non-bonded interactions starts.

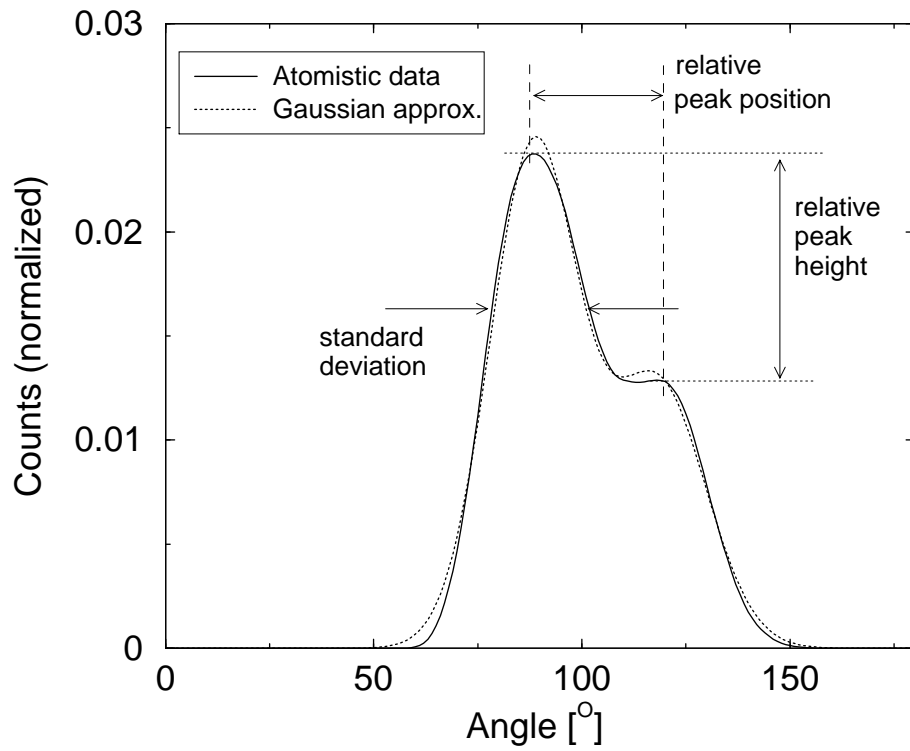


FIG. 11. Bond angle parametrization for the PAA CG model. The atomistic data could be fitted by two Gaussians. This leaves four parameters for the coarse graining optimization: relative peak height, relative peak position and the two standard deviations.

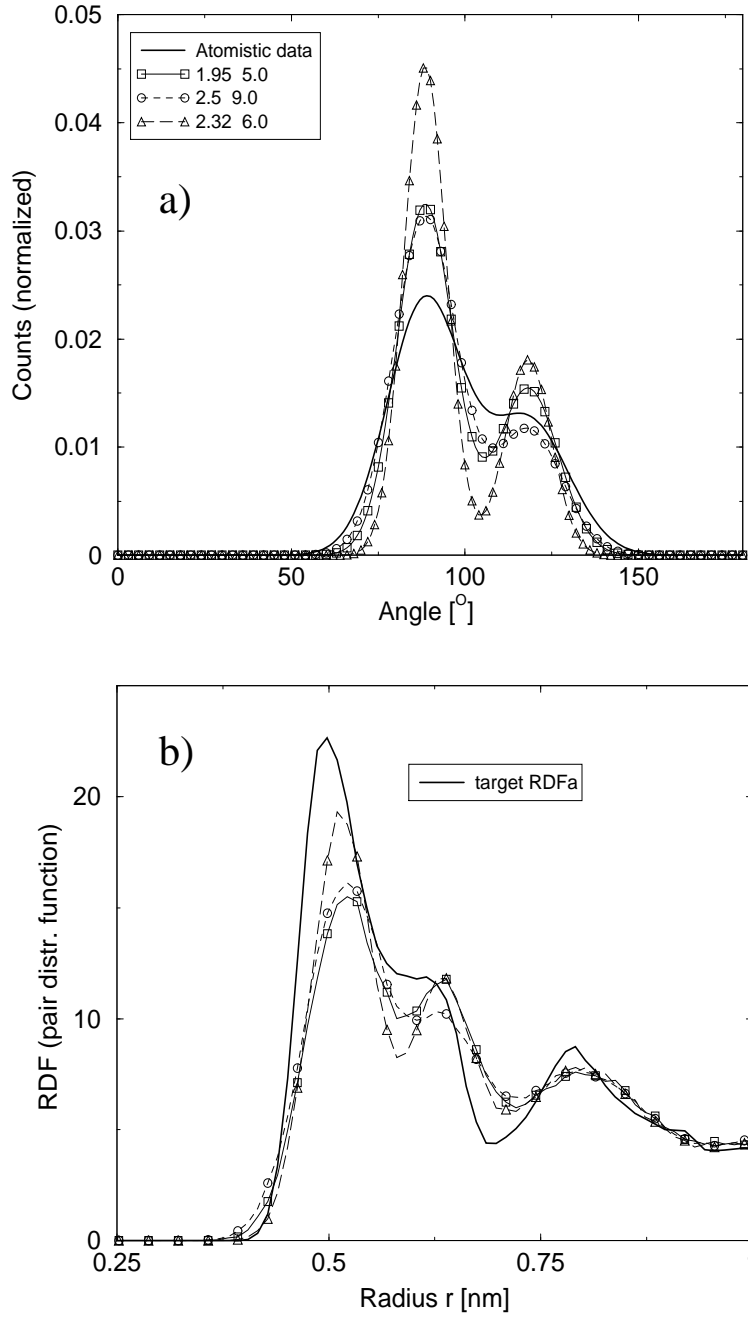


FIG. 12. Bond angle potential optimization against the RDF-a for PAA. (a) Input distributions. The relative amplitudes (first number) and the standard deviation (second number) of the main peak are optimized. (b) The resulting RDF-a. For the non-bonded interactions, a LJ 6-12 potential with $\varepsilon = 0.384$ and $\sigma = 0.74$ is applied.

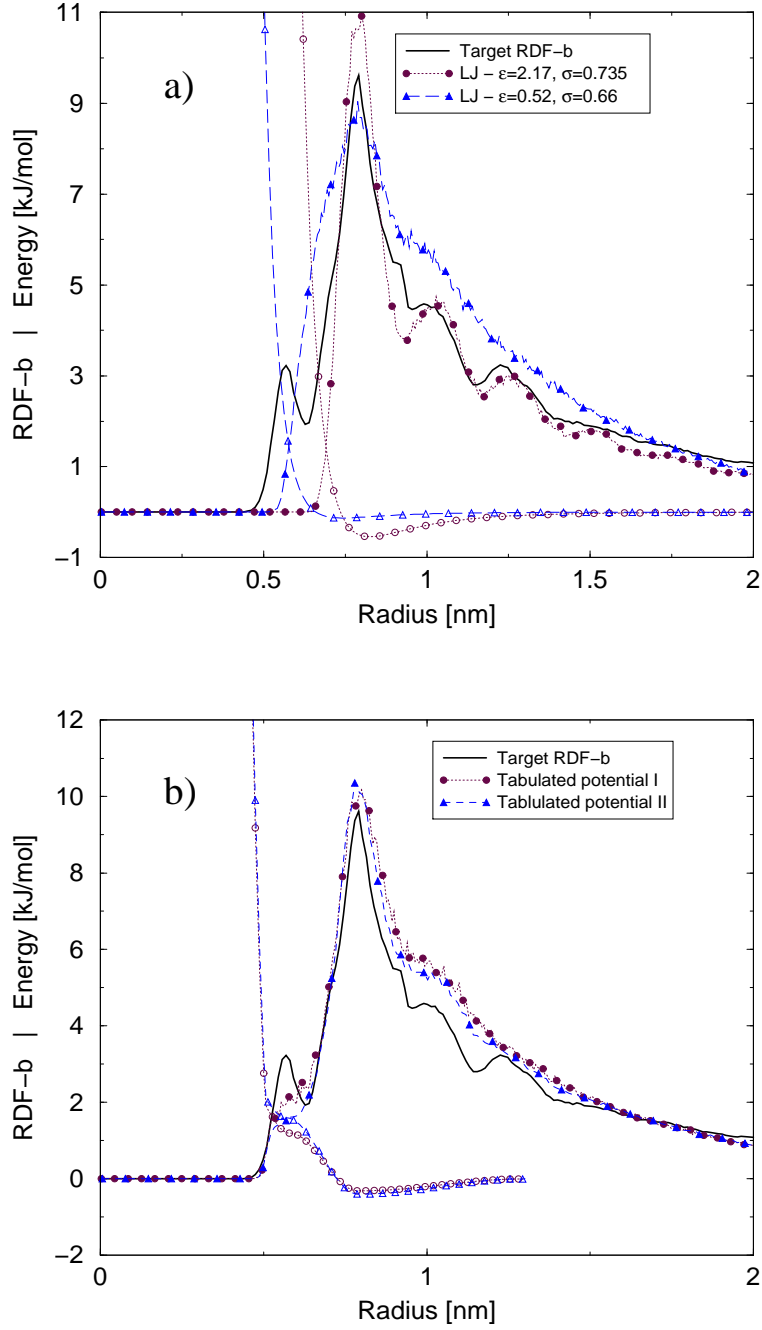


FIG. 13. Non-bonded potential optimization against RDF-b for PAA. Open symbols denote the potentials, filled symbols the corresponding RDFs. Small changes in the potentials manifest themselves strongly in the trial RDFs. (a) Lennard-Jones 6-12 potential of Equation 3.8 (b) Piecewise potential of Equation 3.9

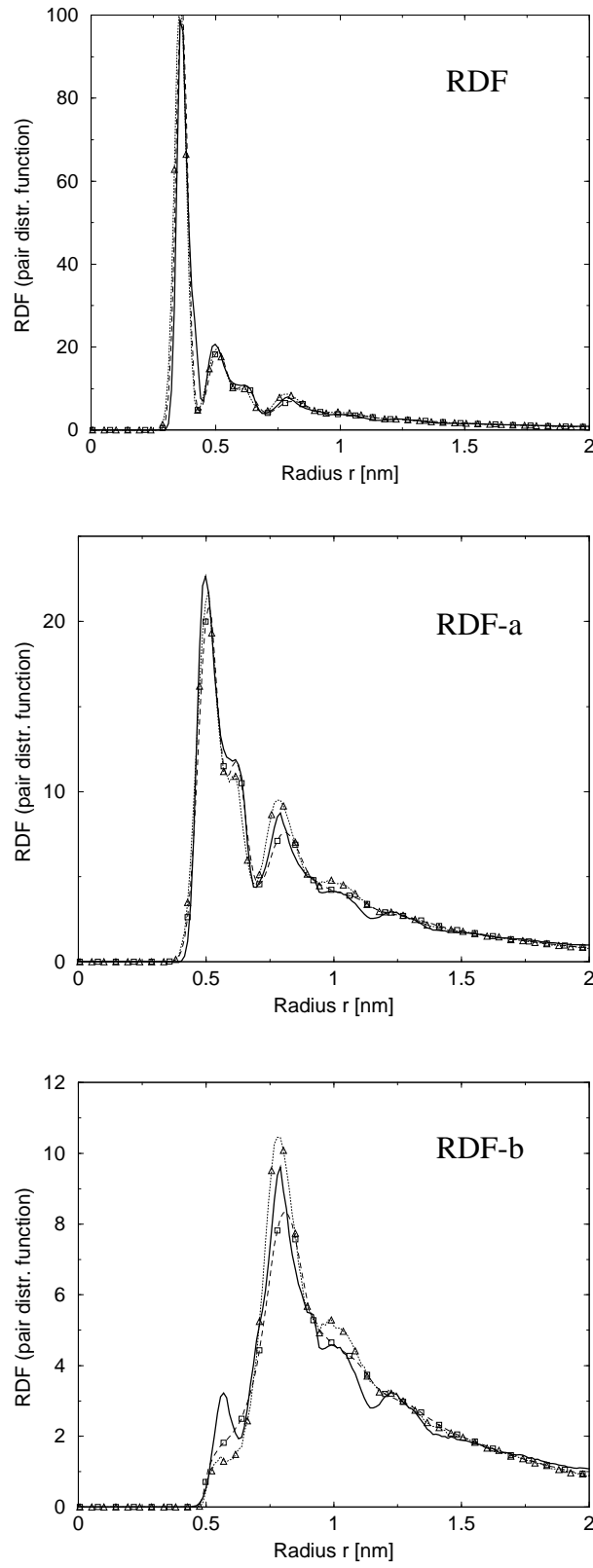


FIG. 14. Final optimization result for PAA. Thick lines: target RDFs from atomistic simulations. Triangles: first optimization force field. Squares: improved force field, including torsions. All features of the RDF are at least qualitatively well reproduced.

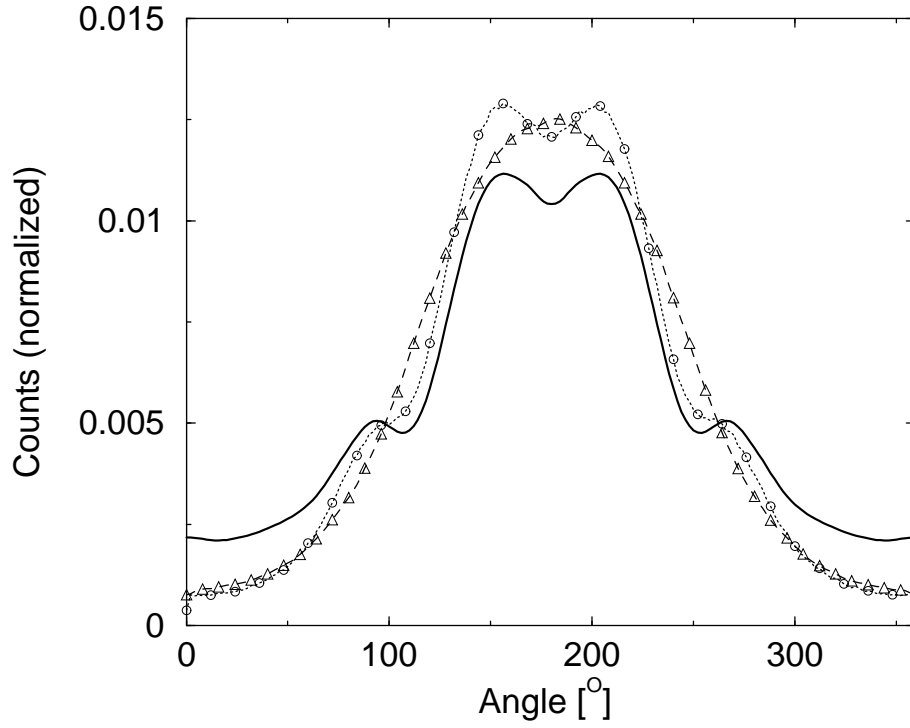


FIG. 15. Normalized distribution of the dihedral angles for PAA, obtained from the simulation. The atomistic data (solid line) is symmetrized and 7-point smoothed. The coarse grained data is obtained for the force fields without (circles) and with (triangles) torsional potential. Qualitatively, they reproduce the atomistic curve but for both, the peak is overrepresented whilst the valley is underrepresented.

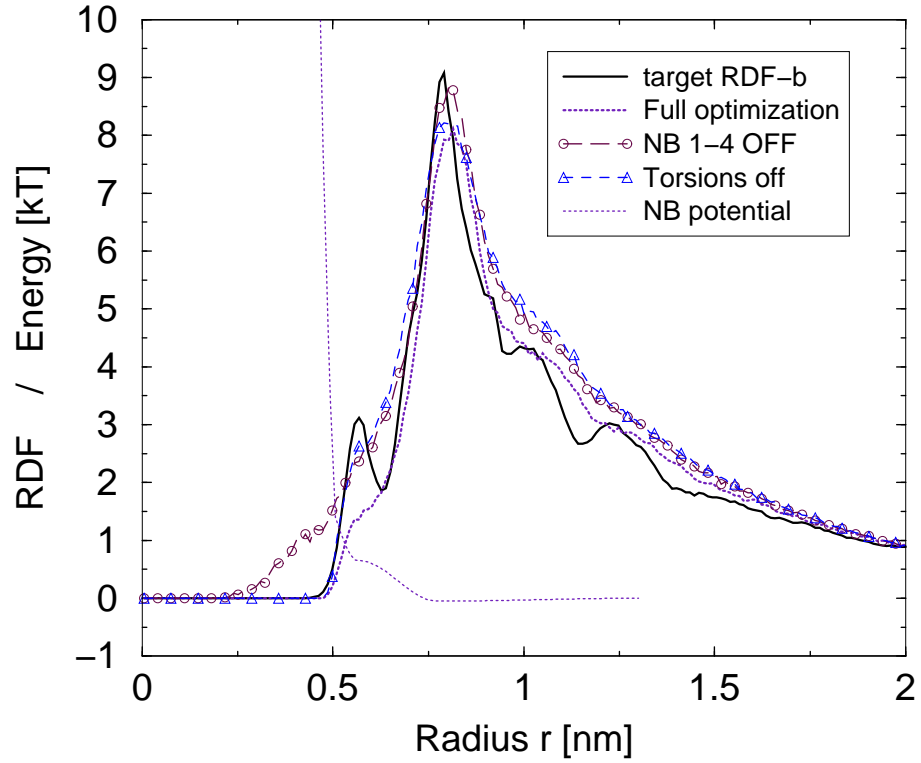


FIG. 16. Interplay of torsional and non-bonded interactions for an RDF-b of PAA. Runs with partly switched off interactions can be compared to the full optimization. Without a non-bonded potential, the ascent starts at too small distances whereas without torsions, the descent is not well reproduced.